Catalysis Science & Technology

On the Active Site for Electrocatalytic Water Splitting on Late Transition Metals Embedded in Graphene

Journal:	*Catalysis Science & Technology*
Manuscript ID	CY-ART-10-2019-002006.R1
Article Type:	Paper
Date Submitted by the Author:	04-Nov-2019
Complete List of Authors:	Kropp, Thomas; University of Wisconsin Madison, Chemical and Biological Engineering Rebarchik, Michael; University of Wisconsin Madison, Chemical and Biological Engineering Mavrikakis, Manos; University of Wisconsin Madison, Chemical and Biological Engineering

On the Active Site for Electrocatalytic Water Splitting on Late Transition Metals Embedded in Graphene

Thomas Kropp,* Michael Rebarchik, and Manos Mavrikakis*

Department of Chemical and Biological Engineering, University of Wisconsin—Madison, 1415 Engineering Drive, Madison, Wisconsin 53706, United States

Abstract: Transition-metal atoms embedded in nitrogen-doped graphene can be used for electrocatalytic water splitting, but there are open questions regarding the identity of the active site. We study the formation of hydrogen and oxygen as well as the reduction of oxygen on 14 transition metals embedded in nitrogen-doped graphene using density functional theory and find that the stability and the catalytic properties of the metals depend on the nitrogen content of the support. While previous studies focus on metal atoms inside nitrogen-free and fully substituted vacancies, we find that partially nitrogen-substituted single sites are significantly more active for later transition metals (group 10-11). These sites are also more stable than previously suggested active-site models. Our findings suggest that stability and catalytic activity of late transition metals embedded in graphene could be increased by controlling the nitrogen content of the support to obtain partially substituted vacancy sites. For early transition metals, fully substituted vacancies represent the most active site.

Keywords: density functional theory, graphene, hydrogen evolution, oxygen evolution, nitrogen-doping, single-atom catalysts

*** Corresponding Authors:**

Thomas Kropp (tekropp@wisc.edu, ORCID 0000-0002-9166-566X) and

Manos Mavrikakis (emavrikakis@wisc.edu, ORCID 0000-0002-5293-5356)

1. Introduction

Hydrogen is considered a clean alternative to fossil fuels, but it is still largely derived from steam-reformed methane. Water electrolysis is a promising alternative to the fossil-fuel-based hydrogen production process.[1-3] The corresponding half-cell reactions, the oxygen evolution reaction (OER) and the hydrogen evolution reaction (HER), are shown for an acidic electrolyte in eqs. 1 and 2, respectively. While platinum-based catalysts are among the most effective ones for these reactions,[4,5] the cost of platinum limits its commercial application.

$$2H_2O \rightarrow O_2 + 4H^+ + 4e^- \quad (1)$$

$$4H^+ + 4e^- \rightarrow 2H_2 \quad (2)$$

In recent years, atomically-dispersed transition metals on nitrogen-doped graphene have gained increased attention as more cost-effective catalysts for water splitting. Such single-atom catalysts have been synthesized using cobalt,[6-10] copper,[11] iron,[12-14] molybdenum,[15] nickel,[16-18] ruthenium,[19] platinum,[20-24] and tungsten.[25,26] While it has been established that transition metals bind to vacancy-type defects in graphene, there is still an active debate regarding the nature of the active site. Early studies[15-17] suggested that metal atoms bind atop single vacancies in graphene, though density functional theory (DFT) calculations[27] indicate that such sites may not be stable under typical synthesis conditions (i.e., annealing in an ammonia atmosphere above 600 °C). Recent work[18,21,22] suggests that the metal atoms instead bind to double vacancies containing up to four N substitutions, though edge sites have also been considered.[28]

Choi *et al.*[29] estimated HER overpotentials from DFT calculations on various single-atom catalysts, though they report weak binding between transition metals and the graphene support, which differs from the findings of other groups.[30,31] Hossain *et al.*[30] calculated HER overpotentials from DFT for transition-metal atoms embedded in fourfold N-substituted double vacancies and performed experimental measurements on selected systems. Their calculations suggest that cobalt is the most active metal for HER, whereas nickel and tungsten atoms embedded in N-doped graphene

are only slightly more active than the metal-free support. This finding seemingly contradicts earlier experimental work,[16-18] which demonstrated high HER activity for Ni atoms embedded in N-doped graphene. Similarly, nickel [18] and platinum [24] atoms embedded in N-doped graphene were found to be active toward the oxygen reduction reaction (ORR), which appears to contradict DFT results.[31] These apparent contradictions indicate that the commonly assumed active-site model may not be appropriate for late transition metals.

To gain further insights regarding the active site for HER, OER, and ORR on graphene-based single-atom catalysts, we study 14 transition metals embedded in single and double vacancies of graphene. By comparing their stability as a function of nitrogen content, we conclude that transition metal atoms preferentially bind to double vacancies. For group 7-9 transition metals, the most stable substitution pattern (i.e., four N atoms) is active toward HER, OER, and ORR. For group 10 and 11 transition metals, a less stable site (metal atoms inside threefold N-substituted double vacancies) is significantly more active. The presence of such sites may resolve the apparent contradiction between computational and experimental work on graphene-based single-atom catalysts. These findings are also in line with recent calculations that show how the N content of the support affects the CO oxidation activity of graphene-based single-atom catalysts [27] and offer significant guidance for the synthesis of active and stable graphene-based single-atom electrocatalysts.

2. Methods

2.1. Computational Details. Spin-polarized calculations were performed using the projector augmented wave (PAW) method [32,33] as implemented in the Vienna *ab initio* simulation package (VASP).[34,35] Exchange–correlation energies were obtained using the functional by Perdew, Burke, and Ernzerhof (PBE) [36] with a plane wave cutoff of 600 eV. Structure optimizations were performed until total energies were converged to 10^{-6} eV, and forces acting on the relaxed ions were below 0.02 eV/Å. Structures were proven to be minima by the absence of imaginary frequencies.

Vibrational frequencies were obtained by diagonalizing a partial, mass-weighted matrix of second derivatives with respect to the three Cartesian degrees of freedom of each atom other than the graphene-based support. This Hessian matrix was obtained by finite differences of the gradients with displacements of ±0.015 Å (central differences).

The graphene films (r_{C-C} = 142 pm) were modeled using a $p(6\times5)$ supercell with a vacuum layer of 15 Å. The Brillouin zone was sampled at 4 × 4 × 1 k points. Gas phase molecules were calculated inside a 12 Å cubic box, using only the Gamma point for the integration of the Brillouin zone. Electronic energy convergence with respect to all calculation parameters was confirmed.

2.2. Reaction Energetics. Gibbs free energies (G in eq. 3) were obtained by adding electronic energies (E_{elec}), zero-point vibrational energies (E_{ZPVE}), and entropy contributions (TS) at 298 K and 0.1 MPa; underlying equations are provided in the supplementary material (eqs. S1-S5). Reaction energies were calculated relative to the computational hydrogen electrode introduced by Nørskov and coworkers [4] (i.e., ΔG = 0 kJ/mol for eq. 2 at 0 V_{RHE}). Herein, the overpotential (η) for HER and OER was estimated by dividing the reaction energy of the most endergonic elementary step (after applying the equilibrium potential U_{eq}) by the charge of an electron (i.e., $\Delta G_{max}/e$).

$$G = E_{elec} + E_{ZPVE} - TS \quad (3)$$

3. Results and Discussion

3.1. Stability of Active Site Models. While numerous active site models have been suggested for graphene-supported transition metals, their stability has not yet been compared as a function of the N content of the support. Herein, we consider metal atoms (Me) inside single vacancies (G-V_{1C}) and double vacancies (G-V_{2C}). N substitutions at the vacancies are denoted as GN_m (m is the number of N atoms per vacancy). We previously discussed the binding energies of metals to these sites and showed that metal cluster growth is not favorable at low coverage,[27] but formation energies are

needed to estimate site distributions. By evaluating metal binding energies and overall formation energies, we can assess the stability of previously suggested active site models and suggest new synthesis targets.

As these single-atom catalysts are typically prepared by annealing in an ammonia atmosphere, we calculate formation energies (ΔE_{form}) relative to gas phase ammonia (eq. 4). Herein, Me_{bulk} refers to a bulk metal atom, and G refers to a pristine graphene layer. The formation energy of $Me/GN_m\text{-}V_{nC}$ depends on the products that are formed by the remaining carbon and hydrogen atoms. We assume that they form the most stable hydrocarbon for the specific hydrogen-to-carbon ratio, though this may not be the case depending on kinetic limitations. We estimate the energy of the hydrocarbons as a linear function of the hydrogen-to-carbon ratio (Fig. S1 in the electronic supplementary information). Based on the mean absolute error of our interpolation, this introduces an uncertainty of 6 kJ/mol per C atom. Due to the uncertainty regarding the hydrocarbon products, we refrain from calculating formation entropies as these critically depend on the number of gas phase molecules.

$$Me_{bulk} + G + mNH_3 \rightarrow Me/GN_m\text{-}V_{nC} + C_{m+n}H_{3m}, \quad (4)$$

Fig. 1 shows the formation energy (ΔE_{form}) as a function of the nitrogen content for both single and double vacancies. In agreement with previous work, we find that N doping stabilizes both single and double vacancies (blue squares connected by dashed lines). However, the dimerization of two single vacancies to form a double vacancy is always exothermic. Since migration barriers of single vacancies are relatively low (ca. 135 kJ/mol),[37] double vacancies are expected to be the more common defect after annealing (synthesis conditions typically exceed 600 °C). Molecular dynamics simulations show that two single vacancies may indeed form a double vacancy, while the reverse reaction is not observed.[38]

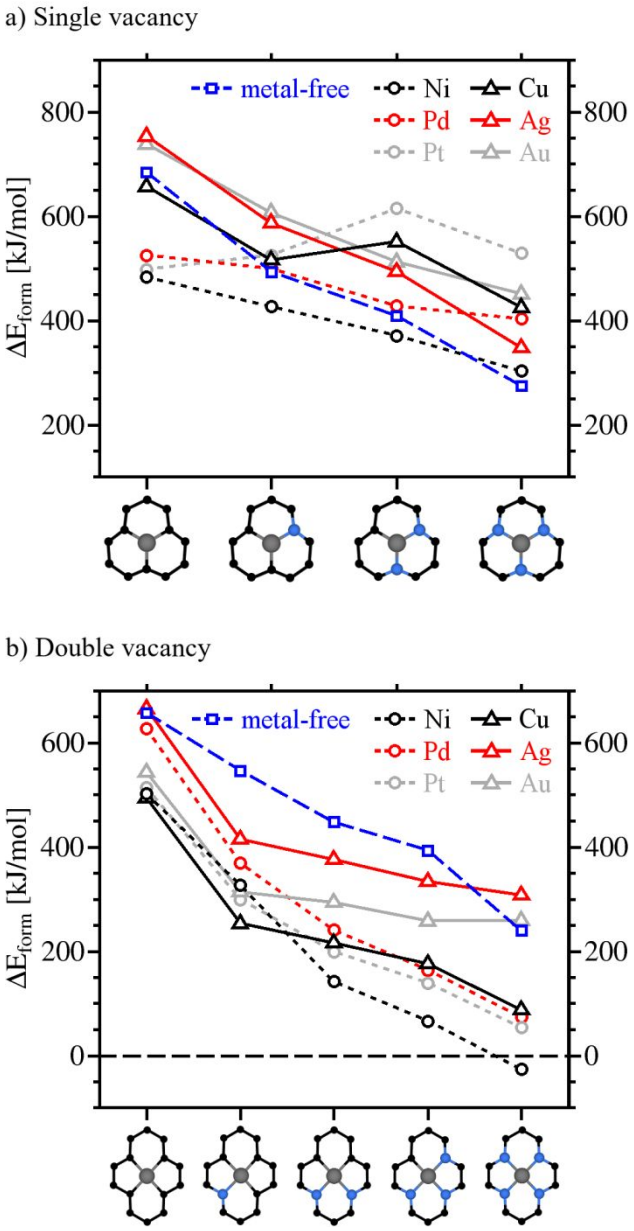

Fig. 1 Formation energies ΔE_{form} (eq. 4) for pristine and metal-decorated (a) single and (b) double vacancies in N-doped graphene; data points are connected to guide the eye. Early transition metals are not included, as they behave qualitatively similar to Ni and Pd. The corresponding graphene vacancy structures are shown below the x-axis, using the following color code: C (black), Me (gray), and N (blue). Raw data is provided in Table 1.

N doping weakens the binding of transition metal atoms to single vacancies (BE_{Me} in Table 1); the positive values indicate that metal particle formation is preferred over atomic dispersion atop single vacancies in N-doped graphene. The more favorable formation energies of metal-decorated single

vacancies at higher N content (Fig. 1a) are solely caused by the lower defect formation energies. Since overall formation energies are substantially endothermic for all transition metals, we conclude that metal-decorated single vacancies are metastable.

Table 1 GN_m-V_{nC} vacancy formation energies (ΔE_{form}[a]) and binding energies of transition-metal atoms (BE_{Me}) inside the vacancy using bulk-metal atoms as the reference. The formation energies plotted in Fig. 1 are obtained by adding vacancy formation energies and the corresponding binding energies. All energies are given in kJ/mol.

	G-V_{1C}	GN_1-V_{1C}	GN_2-V_{1C}	GN_3-V_{1C}	G-V_{2C}	GN_1-V_{2C}	GN_2-V_{2C}	GN_3-V_{2C}	GN_4-V_{2C}
ΔE_{form}	684	493	409	275	657	546	448	393	240
BE_{Ag}	69	94	84	74	-2	-130	-72	-59	68
BE_{Au}	54	114	103	176	-124	-231	-154	-135	19
BE_{Co}	-267	-101	-66	169	-154	-224	-228	-263	-235
BE_{Cr}	-221	-105	-18	32	-29	-157	-180	-255	-246
BE_{Cu}	-28	23	141	150	-173	-292	-232	-218	-152
BE_{Fe}	-235	-96	-42	218	-134	-233	-207	-243	-214
BE_{Ir}	-201	4	131	311	-136	-100	-113	-146	-92
BE_{Mn}	-249	-83	-62	35	-132	-273	-253	-298	-263
BE_{Mo}	-112	56	103	192	-90	4	-47	-62	24
BE_{Ni}	-201	-66	-38	29	-165	-289	-305	-327	-266
BE_{Pd}	-160	7	18	129	-40	-176	-207	-229	-166
BE_{Pt}	-187	32	203	251	-153	-246	-251	-257	-186
BE_{Rh}	-254	-72	10	154	-145	-106	-132	-174	-131
BE_{Ru}	-273	-34	-17	171	-195	-68	-55	-69	-17

[a] $G + mNH_3 \rightarrow GN_m\text{-}V_{nC} + C_{m+n}H_{3m}$.

Ni/GN_3-V_{1C} was recently suggested to be the active site for HER on atomically dispersed nickel,[17] but based on its highly endothermic formation energy and the weak binding of Ni to GN_3-V_{1C} (BE_{Ni} = +29 kJ/mol), we infer that this site is not likely to be present in significant amounts and that the experimentally observed HER activity probably originates from a more stable active site. Interestingly, Qiu *et al.*[16] report TEM images of individual Ni atoms atop N-free single vacancies, though they did not anneal their catalyst. Thus, the presence of metastable Ni/G-V_{1C} is likely the result of their synthesis approach (i.e., graphene growth on metallic Ni followed by dissolution of metallic

Ni in acid). Since most transition metals bind strongly to N-free single vacancies (Table 1), this synthesis strategy can likely be used to obtain other Me/G-V_{1C} catalysts.

As previously reported,[27] all transition metals other than Mo bind strongly to N-substituted double vacancies. Here, the metal atoms bind in the graphene plane. Correspondingly, the metal *d* orbitals can strongly interact with the N *p* orbitals. However, metal atoms cannot fit inside the single vacancies and adsorb atop the vacancy, leading to this qualitatively different behavior. For period 4 elements (Cr, Mn, Fe, Co, Ni, Cu), the metal binding energy is similar to the formation energy of a fully N-substituted double vacancy, so the formation of Me/GN_4-V_{2C} becomes exothermic, which is shown for Ni in Fig. 1b. However, the formation energy of Me/GN_3-V_{2C} is within 100 kJ/mol off the fully substituted vacancy. This is due to metal–support interactions being stronger for partially substituted double vacancies (Table 1). Since entropic and kinetic effects may favor Me/GN_3-V_{2C}, these partially substituted double vacancies could be present depending on the synthesis conditions. In the following sections, we will study the activity of Me/GN_3-V_{2C} and Me/GN_4-V_{2C} toward HER, OER, and ORR.

3.2. Hydrogen Evolution. Previous computational studies [30,31] suggest that hydrogen evolution on graphene-based single-atom catalysts follows a two-step mechanism: A proton-electron pair forms a H* species (eq. 5; the asterisk indicates an adsorbed species), which then reacts with a second proton-electron pair to form molecular hydrogen (eq. 6). While transition metal atoms inside larger vacancies can strongly bind multiple H atoms,[39] hydrogen formation is more favorable than the co-adsorption of two H* on Me/GN_m-V_{2C}. The overpotential is estimated by dividing the absolute value of the Gibbs free adsorption energy of ½ H_2 by the charge of an electron.

$$(H^+ + e^-) + * \rightarrow H^* \quad (5)$$

$$(H^+ + e^-) + H^* \rightarrow H_2 + * \quad (6)$$

Fig. 2 shows the calculated HER overpotential (η_{HER}) as a function of the electronic H binding energies relative to ½ H_2 (BE_H); the data is also compiled in Table S1. Based on our fit (R^2 = 0.99), the ideal HER catalyst should have a hydrogen affinity of BE_H = -27 kJ/mol, which is within 3 kJ/mol of previous computational studies.[30,31] In contrast to previous studies that estimate Gibbs free energies from electronic energies using a correction factor that was obtained for extended metal surfaces,[40] we report Gibbs free energies that are calculated from *ab initio* frequencies. Nonetheless, HER overpotentials reported herein are within 0.1 V of previously reported values, validating the approximations used in the previous studies.

Co/GN_4-V_{2C} and Rh/GN_4-V_{2C} (abbreviated as Co-N_4 and Rh-N_4 in Fig. 2a) are predicted to be particularly active HER catalysts with overpotentials of 0.2 and 0.1 V, respectively. The reaction intermediates on Co/GN_4-V_{2C} are shown in Fig. 2b, and adsorption structures on other transition metals are similar. For cobalt, the estimated overpotential (0.2 V) is in good agreement with the experimentally observed onset potential of 0.15 V 7. However, HER overpotentials on late transition metals inside fourfold substituted double vacancies (blue circles in Fig. 2a) are predicted to be prohibitively large. While metallic Pt has a H affinity (BE_H = -40 kJ/mol in ref 41) close to the ideal value (-27 kJ/mol), Pt/GN_4-V_{2C} is predicted to be inactive toward HER (BE_H = 115 kJ/mol). The active site corresponding to the experimentally observed HER activity of late transition metals embedded in N-doped graphene [16-18] has not yet been conclusively identified.

We find that metal atoms inside partially substituted double vacancies bind hydrogen more strongly than those inside fourfold substituted ones, as H may bind in a bridging configuration atop the Me–C bond (Fig. 2c). For late transition metals inside GN_3-V_{2C} (abbreviated as Me-N_3 in Fig. 2a), H binding energies are close to the ideal value, which leads to high HER activity on these sites. Cu/GN_3-V_{2C} and Ni/GN_3-V_{2C} are particularly active with overpotentials of 0.1 and 0.2 V, respectively. Metal atoms inside double vacancies with an even lower N content bind H atoms more strongly, which lowers their HER activity. This is shown for Ni in Fig. S2. The H affinity of early transition

metals increases similarly, when the N content of the support decreases, lowering the HER activity. For these metals, the fully N-substituted double vacancy is predicted to be the most active site.

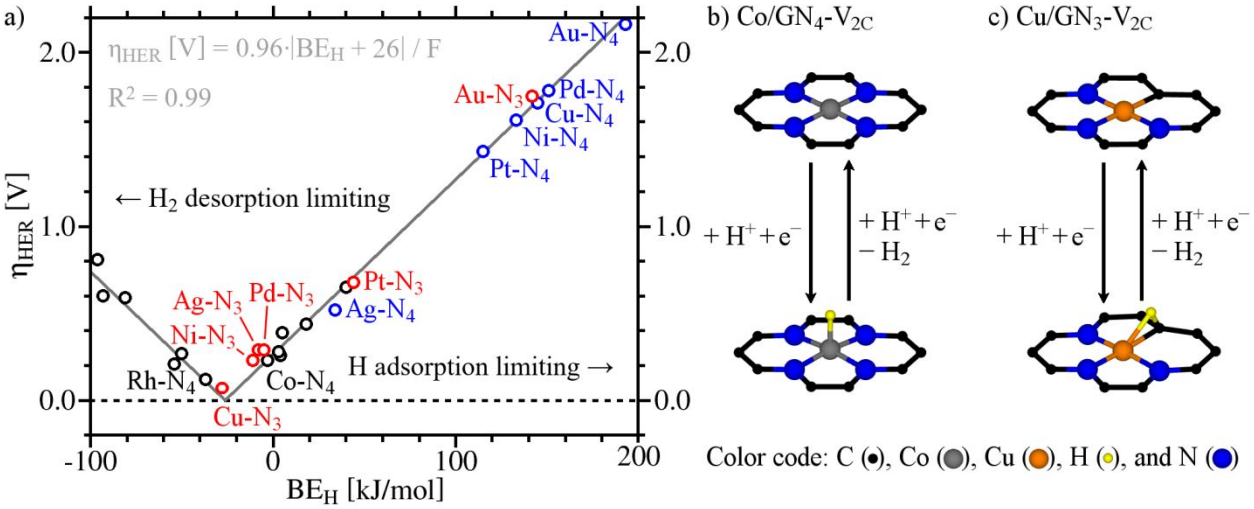

Fig. 2 (a) Calculated overpotential for HER (η_{HER}) on transition-metal atoms embedded in N-doped graphene as a function of the H atom binding energy relative to ½ H_2, i.e. BE_H. The linear fit has a minimum at BE_H = -27 kJ/mol and a mean absolute error (MAE) of 0.02 V. The corresponding intermediate structures on (b) Co/GN_4-V_{2C} and (c) Cu/GN_3-V_{2C} are shown as tilted side views. Black labels refer to early transition metals, whereas late transition metals are highlighted using blue (Me/GN_4-V_{2C}) and red (Me/GN_3-V_{2C}) labels.

3.3. Oxygen Evolution Reaction. Previous computational work suggests that oxygen reduction follows the associative mechanism on graphene-based single-atom catalysts.[31] We therefore assume that oxygen evolution follows the reverse mechanism on these catalysts (eqs. 7-11). After applying the equilibrium potential obtained using PBE (i.e., +1.07 V and -1.07 V for ORR and OER, respectively), the overpotential is estimated by dividing the reaction energy of the most endergonic step by the charge of an electron.

$$H_2O + * \rightarrow (H^+ + e^-) + OH^* \quad (7)$$

$$OH^* \rightarrow (H^+ + e^-) + O^* \quad (8)$$

$$H_2O + O^* \rightarrow (H^+ + e^-) + O_2H^* \quad (9)$$

$$O_2H^* \rightarrow (H^+ + e^-) + O_2^* \quad (10)$$

$$O_2^* \rightarrow O_2 + * \qquad (11)$$

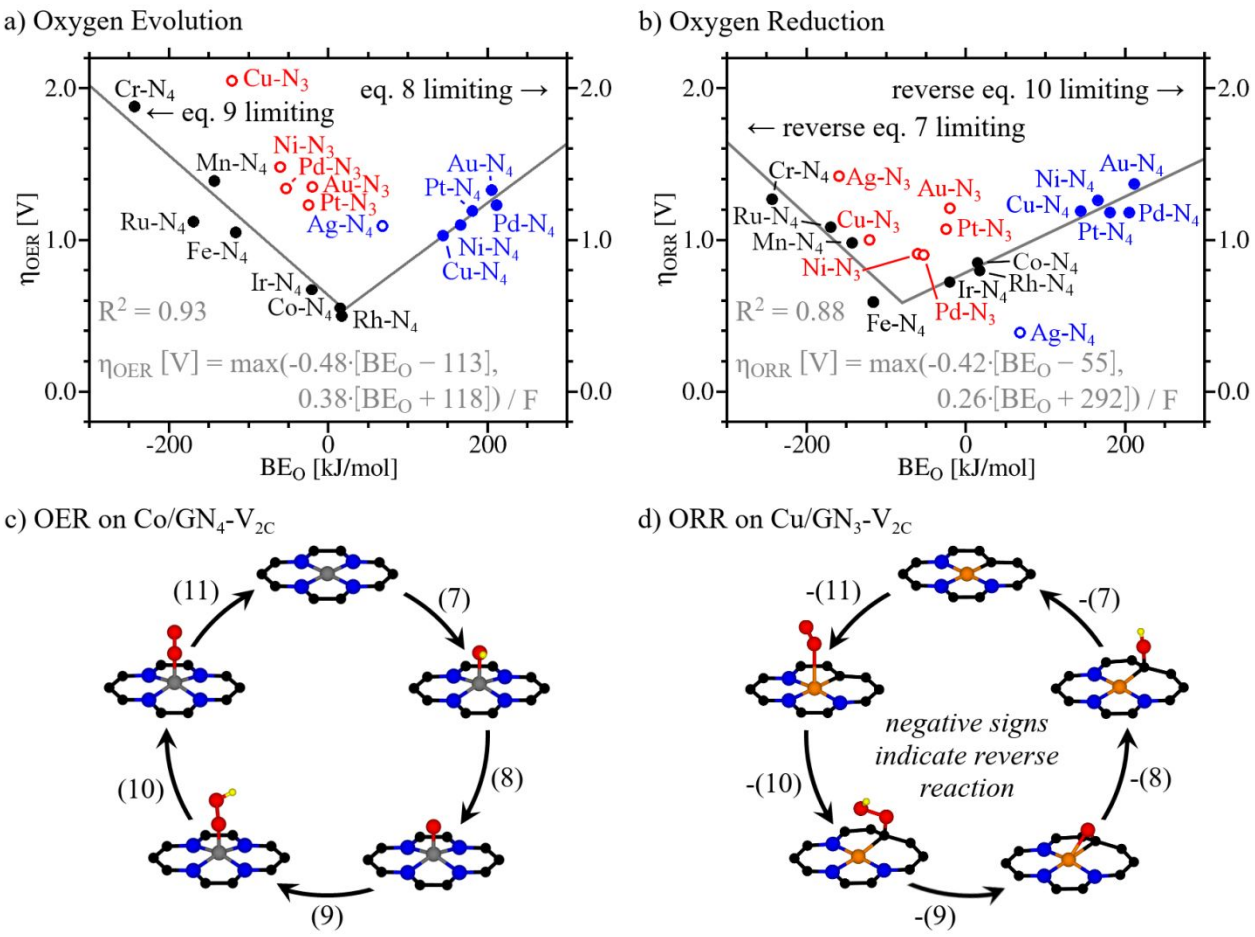

Fig. 3 Calculated overpotentials for (a) OER (η_{OER}) and (b) ORR (η_{ORR}) on transition-metal atoms in N-doped graphene as a function of O binding energies relative to ½ O_2 (BE_O). Black labels refer to early transition metals, whereas late transition metals are highlighted using blue (Me/GN_4-V_{2C}) and red (Me/GN_3-V_{2C}) labels. The linear fits (solid circles only) for OER (MAE = 0.07 V) and ORR (MAE = 0.07 V) have minima at BE_O values of +11 and -77 kJ/mol, respectively. The corresponding intermediates on (c) Co/GN_4-V_{2C} and (d) Cu/GN_3-V_{2C} are shown as side views using the same color code as Fig. 2; i.e., C (black), Co (gray), Cu (orange), H (yellow), N (blue), and O (red).

Fig. 3a shows the calculated OER overpotential (η_{OER}) as a function of the O binding energy relative to ½ O_2. Due to the instability of Ag/GN_4-V_{2C} and Mo/GN_4-V_{2C} (positive Me binding energies in Table 1), both were treated as outliers when calculating linear fits. Based on our fit (R^2 = 0.93), the ideal OER catalyst should have an electronic O binding energy of 11 kJ/mol. On more oxophilic

catalysts (Cr, Fe, Ir, Mn, and Ru atoms in GN_4-V_{2C}), the formation of the peroxo species (eq. 9) is predicted to be potential-limiting, whereas the dehydrogenation of the OH* species (eq. 8) is potential-limiting on less oxophilic catalysts (Ag, Au, Co, Cu, Rh, Ni, Pd, and Pt atoms in GN_4-V_{2C}). Individual reaction energies for eqs. 7-11 are compiled in Table S1; spin states of reaction intermediates are compiled in Table S2. Reaction intermediates on the Co catalyst are shown in Fig. 3c, though intermediates on other transition metals are similar. Co/GN_4-V_{2C} and Rh/GN_4-V_{2C} (abbreviated as Co-N_4 and Rh-N_4 in Fig. 3a) are predicted to be particularly active OER catalysts with overpotentials below 0.6 V.

Fig. 3b shows the calculated ORR overpotential (η_{ORR}) as a function of the O binding energy. Based on our linear fit (R^2 =0.88), the ideal ORR catalyst should be more oxophilic than the ideal OER catalyst with an O binding energy of -77 kJ/mol, which is close to the ideal value on extended metal surfaces (-62 kJ/mol from PW91,[4] O binding energies on metallic surfaces obtained using PW91 and PBE are within 26 kJ/mol in ref 41). On more oxophilic catalysts (Cr, Fe, Mn, and Ru atoms in GN_4-V_{2C}), the second water formation step (reverse eq. 7, which is indicated by a negative sign in Fig. 3d) is predicted to be potential-limiting, whereas O_2 activation (reverse eq. 11) is potential-limiting on less oxophilic catalysts (Ag, Au, Co, Cu, Ir, Rh, Ni, Pd, and Pt atoms in GN_4-V_{2C}). Fe/GN_4-V_{2C} and Ir/GN_4-V_{2C} (abbreviated as Fe-N_4 and Ir-N_4 in Fig. 3b) are predicted to be particularly active ORR catalysts with overpotentials of 0.6 and 0.7 V, respectively. We note that co-adsorbed O species were suggested to lead to an increase in the ORR activity of Fe [14] and Ru [19] single-atom catalysts. However, coverage effects are not likely to affect the activity of late transition metals (Au, Cu, Ni, Pd, and Pt) due to their low oxygen affinity, i.e. having more than one O atom per metal atom is highly unlikely.

Overpotentials for OER and ORR on late transition metals inside fourfold-substituted double vacancies are prohibitively large (blue circles in Figs. 3a-b), whereas experimental studies report significant ORR activity on copper [11] and platinum [24] single-atom catalysts. Based on their O binding energies, partially N-substituted vacancies are predicted to be more active, but our calculations

indicate that Me/GN_3-V_{2C} is not necessarily more active than the fully N-substituted model, as the overpotentials (red circles in Figs. 3a-b) deviate significantly from the scaling relations that were calculated for metal atoms inside fully substituted double vacancies. This is due to different adsorption sites of the O_mH_n species.

On Me/GN_4-V_{2C}, all intermediates bind atop the metal ions (Fig. 3c), but different binding modes are preferred on Me/GN_3-V_{2C} (Fig. 3d): while OH* and OOH* bind to the C atom in the vicinity of the metal atom, atomic O binds in a bridging configuration on the Me–C bond, and molecular O_2 binds atop the metal atom. Since atomic O is more strongly stabilized than the OOH* species, eq. 9 is more endothermic than the scaling relations would indicate, lowering the OER activity of the partially substituted sites. While Me/GN_3-V_{2C} is predicted to be more active toward ORR than Me/GN_4-V_{2C} (Fig. 3b), the relatively large overpotentials indicate that the experimentally observed ORR activity might result from even more active sites such as metal atoms inside larger vacancies (Me/GN_m-V_{nC} with n > 2). For example, an ORR overpotential of 0.6 V has been reported for Cu/GN_6-V_{6C}.[42]

4. Conclusions

We study electrocatalytic water splitting on transition-metal atoms embedded in nitrogen-doped graphene using density functional theory and find that the stability and the catalytic properties of the metals depend on the nitrogen content of the support. While previous studies focus on metal atoms inside nitrogen-free and fully substituted vacancies, we find that partially nitrogen-substituted single sites are significantly more active toward HER for later transition metals (group 10-11). While partially substituted sites are also more active toward ORR, atomic descriptors overestimate their catalytic OER and ORR activity as these sites deviate from the scaling relations developed for fully substituted sites. For early transition metals, fully N-substituted double vacancies are the most active site for all the reactions studied herein. Overall, our findings indicate that the catalytic activity of late transition metal atoms embedded in graphene can be increased by controlling the nitrogen content

of the support towards intermediate values, while a higher nitrogen content is desirable for early transition metals. These findings may also resolve the apparent contradiction between computational and experimental studies regarding the catalytic activity of atomically dispersed late transition metals on graphene.

Electronic Supplementary Information

Further equations; electronic energy of small organic molecules; HER overpotential on $Ni/GN_m\text{-}V_{2C}$ as a function of the nitrogen content; HER, OER, and ORR energetics.

Conflicts of Interest

The authors declare no competing financial interest.

Acknowledgements

This work has been supported by the U.S. Department of Energy (DOE) through the Office of Basic Energy Sciences (BES); grant number DE-FG02-05ER15731. Computational work was performed using supercomputing resources at the National Energy Research Scientific Computing Center (NERSC) under contract number DE-AC02-05CH11231, at the Center for Nanoscale Materials (CNM) at Argonne National Laboratory under contract number DE-AC02-06CH11357, and at the UW–Madison Center for High Throughput Computing (CHTC). CHTC is supported by UW-Madison, the Advanced Computing Initiative, the Wisconsin Alumni Research Foundation, the Wisconsin Institutes for Discovery, and the National Science Foundation. T. Kropp is grateful for partial financial support by the Alexander von Humboldt Foundation. We thank J. Gold and S. Tacey for helpful comments on the manuscript.

References

1. N. S. Lewis and D. G. Nocera, *Proc. Natl. Acad. Sci. USA*, 2006, 103, 15729.
2. M. G. Walter, E. L. Warren, J. R. McKone, S. W. Boettcher, Q. Mi, E. A. Santori and N. S. Lewis, *Chem. Rev.*, 2010, 110, 6446-6473.
3. Y. Jiao, Y. Zheng, M. Jaroniec and S. Z. Qiao, *Chem. Soc. Rev.*, 2015, 44, 2060-2086.
4. J. K. Nørskov, J. Rossmeisl, A. Logadottir, L. Lindqvist, J. R. Kitchin, T. Bligaard and H. Jónsson, *J. Phys. Chem. B*, 2004, 108, 17886-17892.
5. J. K. Nørskov, T. Bligaard, J. Rossmeisl and C. H. Christensen, *Nat. Chem.*, 2009, 1, 37.
6. H. Fei, J. Dong, M. J. Arellano-Jiménez, G. Ye, N. Dong Kim, E. L. G. Samuel, Z. Peng, Z. Zhu, F. Qin, J. Bao, M. J. Yacaman, P. M. Ajayan, D. Chen and J. M. Tour, *Nat. Commun.*, 2015, 6, 8668.
7. H.-W. Liang, S. Brüller, R. Dong, J. Zhang, X. Feng and K. Müllen, *Nat. Commun.*, 2015, 6, 7992.
8. P. Sabhapathy, C.-C. Liao, W.-F. Chen, T.-C. Chou, I. Shown, A. Sabbah, Y.-G. Lin, J.-F. Lee, M.-K. Tsai, K.-H. Chen and L.-C. Chen, *J. Mater. Chem. A*, 2019, 7, 7179-7185.
9. L. Cao, Q. Luo, W. Liu, Y. Lin, X. Liu, Y. Cao, W. Zhang, Y. Wu, J. Yang, T. Yao and S. Wei, *Nat. Catal.*, 2019, 2, 134-141.
10. J. Wu, H. Zhou, Q. Li, M. Chen, J. Wan, N. Zhang, L. Xiong, S. Li, B. Y. Xia, G. Feng, M. Liu and L. Huang, *Adv. Energy Mater.*, 2019, 9, 1900149.
11. L. Cui, L. Cui, Z. Li, J. Zhang, H. Wang, S. Lu and Y. Xiang, *J. Mater. Chem. A*, 2019, DOI: 10.1039/C9TA03518D.
12. A. Zitolo, V. Goellner, V. Armel, M.-T. Sougrati, T. Mineva, L. Stievano, E. Fonda and F. Jaouen, *Nat. Mater.*, 2015, 14, 937-942.
13. H. T. Chung, D. A. Cullen, D. Higgins, B. T. Sneed, E. F. Holby, K. L. More and P. Zelenay, *Science*, 2017, 357, 479.
14. X. Chen, L. Yu, S. Wang, D. Deng and X. Bao, *Nano Energy*, 2017, 32, 353-358.
15. W. Chen, J. Pei, C.-T. He, J. Wan, H. Ren, Y. Zhu, Y. Wang, J. Dong, S. Tian, W.-C. Cheong, S. Lu, L. Zheng, X. Zheng, W. Yan, Z. Zhuang, C. Chen, Q. Peng, D. Wang and Y. Li, *Angew. Chem. Int. Ed.*, 2017, 56, 16086-16090.
16. H. J. Qiu, Y. Ito, W. Cong, Y. Tan, P. Liu, A. Hirata, T. Fujita, Z. Tang and M. Chen, *Angew. Chem. Int. Ed.*, 2015, 54, 14031-14035.
17. Q. Zhao, J. Sun, S. Li, C. Huang, W. Yao, W. Chen, T. Zeng, Q. Wu and Q. Xu, *ACS Catal.*, 2018, 8, 11863-11874.
18. L. Zhang, Y. Jia, G. Gao, X. Yan, N. Chen, J. Chen, M. T. Soo, B. Wood, D. Yang, A. Du and X. Yao, *Chem*, 2018, 4, 285-297.
19. C. Zhang, J. Sha, H. Fei, M. Liu, S. Yazdi, J. Zhang, Q. Zhong, X. Zou, N. Zhao, H. Yu, Z. Jiang, E. Ringe, B. I. Yakobson, J. Dong, D. Chen and J. M. Tour, *ACS Nano*, 2017, 11, 6930-6941.
20. N. Cheng, S. Stambula, D. Wang, M. N. Banis, J. Liu, A. Riese, B. Xiao, R. Li, T.-K. Sham, L.-M. Liu, G. A. Botton and X. Sun, *Nat. Commun.*, 2016, 7, 13638.
21. T. Li, J. Liu, Y. Song and F. Wang, *ACS Catal.*, 2018, 8, 8450-8458.
22. H. Zhang, P. An, W. Zhou, B. Y. Guan, P. Zhang, J. Dong and X. W. Lou, *Sci. Adv.*, 2018, 4, eaao6657.
23. S. Ye, F. Luo, Q. Zhang, P. Zhang, T. Xu, Q. Wang, D. He, L. Guo, Y. Zhang, C. He, X. Ouyang, M. Gu, J. Liu and X. Sun, *Energy Environ. Sci.*, 2019, 12, 1000-1007.

24. J. Liu, M. Jiao, B. Mei, Y. Tong, Y. Li, M. Ruan, P. Song, G. Sun, L. Jiang, Y. Wang, Z. Jiang, L. Gu, Z. Zhou and W. Xu, *Angew. Chem. Int. Ed.*, 2019, 58, 1163-1167.
25. W. Chen, J. Pei, C.-T. He, J. Wan, H. Ren, Y. Wang, J. Dong, K. Wu, W.-C. Cheong, J. Mao, X. Zheng, W. Yan, Z. Zhuang, C. Chen, Q. Peng, D. Wang and Y. Li, *Adv. Mater.*, 2018, 30, 1800396.
26. Z. Chen, W. Gong, Z. Liu, S. Cong, Z. Zheng, Z. Wang, W. Zhang, J. Ma, H. Yu, G. Li, W. Lu, W. Ren and Z. Zhao, *Nano Energy*, 2019, 60, 394-403.
27. T. Kropp and M. Mavrikakis, *ACS Catal.*, 2019, 9, 6864-6868.
28. G. Gao, S. Bottle and A. Du, *Catal. Sci. Technol.*, 2018, 8, 996-1001.
29. C. Choi, S. Back, N.-Y. Kim, J. Lim, Y.-H. Kim and Y. Jung, *ACS Catal.*, 2018, 8, 7517-7525.
30. M. D. Hossain, Z. Liu, M. Zhuang, X. Yan, G.-L. Xu, C. A. Gadre, A. Tyagi, I. H. Abidi, C.-J. Sun, H. Wong, A. Guda, Y. Hao, X. Pan, K. Amine and Z. Luo, *Adv. Energy Mater.*, 2019, 9, 1803689.
31. S. Back, A. R. Kulkarni and S. Siahrostami, *ChemCatChem*, 2018, 10, 3034-3039.
32. P. E. Blöchl, *Phys. Rev. B*, 1994, 50, 17953-17979.
33. G. Kresse and D. Joubert, *Phys. Rev. B*, 1999, 59, 1758-1775.
34. G. Kresse and J. Furthmüller, *Phys. Rev. B*, 1996, 54, 11169-11186.
35. G. Kresse and J. Furthmüller, *Comput. Mater. Sci.*, 1996, 6, 15-50.
36. J. P. Perdew, K. Burke and M. Ernzerhof, *Phys. Rev. Lett.*, 1996, 77, 3865-3868.
37. A. V. Krasheninnikov, P. O. Lehtinen, A. S. Foster and R. M. Nieminen, *Chem. Phys. Lett.*, 2006, 418, 132-136.
38. G.-D. Lee, C. Z. Wang, E. Yoon, N.-M. Hwang, D.-Y. Kim and K. M. Ho, *Phys. Rev. Lett.*, 2005, 95, 205501.
39. G. Vilé, D. Albani, M. Nachtegaal, Z. Chen, D. Dontsova, M. Antonietti, N. López and J. Pérez-Ramírez, *Angew. Chem. Int. Ed.*, 2015, 54, 11265-11269.
40. J. K. Nørskov, T. Bligaard, A. Logadottir, J. R. Kitchin, J. G. Chen, S. Pandelov and U. Stimming, *J. Electrochem. Soc.*, 2005, 152, J23-J26.
41. J. Wellendorff, T. L. Silbaugh, D. Garcia-Pintos, J. K. Nørskov, T. Bligaard, F. Studt, C. T. Campbell, *Surf. Sci.*, 2015, 640, 36-44.
42. A. M. Patel, S. Ringe, S. Siahrostami, M. Bajdich, J. K. Nørskov, A. R. Kulkarni, *J. Phys. Chem. C*, 2018, 122, 29307-29318.

Graphical Abstract